

**NEUTRON FLUX MEASUREMENTS WITH MONTE CARLO VERIFICATION
AT THE THERMAL COLUMN OF A TRIGA MARK II REACTOR:
FEASIBILITY STUDY FOR A BNCT FACILITY**

EID MAHMOUD EID ABDEL_MUNEM

UNIVERSITI SAINS MALAYSIA

2008

**NEUTRON FLUX MEASUREMENTS WITH MONTE CARLO VERIFICATION
AT THE THERMAL COLUMN OF A TRIGA MARK II REACTOR:
FEASIBILITY STUDY FOR A BNCT FACILITY**

by

EID MAHMOUD EID ABDEL_MUNEM

**Thesis submitted in fulfillment of the
requirements for the degree of
Doctor of Philosophy**

January 2008



ACKNOWLEDGEMENTS

All the praises and thanks are to ALLAH, the Lord of mankind, jinn, and all that exists.

I would like to acknowledge School of Physics, Universiti Sains Malaysia for giving me the opportunity to do this research and for the Malaysian Nuclear Agency (Formerly known as MINT) for their financial support of this research and for the use of their facilities. Special thanks for my main supervisor Prof. Ahmad Shukri for his kind guidance through this research and for his valuable advises. I would like to thank my supervisor Prof. Abdul Aziz Tajuddin for his contributions and ideas. Also thanks to Professor C. S. Chong for the useful discussions and suggestions. I will never forget the motivation and support of Dr. Sabar Bauk.

In addition, I would like to address my thanks to Puan Faridah Mohd Idris from the Malaysian Nuclear Agency for her guidance and support especially at the beginning of the research. My warm thanks and appreciations to Mr. Ahmad Al-Zoubi, Mr. Mahmoud Jawarneh and Mr. Alaa Abdul_Raof for their valuable help and time spent in reading, typing and printing. I deeply appreciate the cooperation of the staff at School of Physics especially Mr. Yahaya Ibrahim, Mr. Azmi Omar, Mr. Burhanuddin Wahi, Mr. Azmi Abdullah junior and the others.

If I forget, I will not forget the motivation and support of my wife, brothers and sisters, and all my friends.

The first and sole motivators for my Ph.D. passed peacefully before this work comes true, May Allah shower my parents with his mercy, and accept them in paradise.

TABLE OF CONTENTS

	Page
ACKNOWLEDGEMENTS	iii
TABLE OF CONTENTS	iv
LIST OF TABLES	ix
LIST OF FIGURES	xii
LIST OF PLATES	xvii
LIST OF APPENDICES	xviii
ABSTRAK	xix
ABSTRACT	xxi
CHAPTER 1 : INTRODUCTION	1
CHAPTER 2 : INTRODUCTORY REVIEW	5
2.1 BNCT - historical review	5
2.2 Theory of BNCT	5
2.3 Neutron energy and BNCT	6
2.4 BNCT - Increased interest and more facilities	9
2.5 The SAND-II choice	10
2.6 Monte Carlo technique	12
2.7 Head phantom and BNCT dosimetry	13
CHAPTER 3: NEUTRON BEAM MEASUREMENTS USING FOIL ACTIVATION METHOD	14
3.1 TRIGA Mark-II reactor	14
3.1.1 Graphite thermal column	14
3.2 Measurement of the neutron flux density in the thermal column	17
3.2.1 Selection criteria of activation foils	17
3.2.2 Foil energy-response	19
3.2.3 Foil testing	19
3.2.4 Foils used in experimental work	20
3.2.4.1 Aluminum (Al)	21
3.2.4.2 Arsenic (As)	23
3.2.4.3 Gold (Au)	23
3.2.4.4 Cobalt (Co)	24

3.2.4.5	Indium (In)	24
3.2.4.6	Molybdenum (Mo)	26
3.2.4.7	Nickel (Ni)	28
3.2.4.8	Rhenium (Re)	29
3.2.4.9	Cadmium (Cd)	30
3.2.5	Product isotope's gamma emission peaks	30
3.3	Experimental setup	31
3.3.1	Pre-irradiation calculations	31
3.3.2	Sample preparation	31
3.3.3	Sample irradiation	35
3.3.4	Gamma ray detection	37
3.3.4.1	Nal(Tl) radiation detector	38
3.3.4.2	HPGe radiation detector	41
3.3.4.3	Efficiency of radiation detectors	42
3.3.4.3.1	Absolute efficiency	43
3.3.4.3.2	Intrinsic efficiency	46
3.3.4.4	Background radiation	48
3.3.4.5	Effect of irradiated polyethylene vial on counting	49
3.3.5	Data processing	52
3.3.6	Saturation activity calculation	56
3.3.6.1	Self shielding and neutron flux depression	57
3.4	Error propagation	58
 CHAPTER 4: ANALYSIS OF NEUTRON SPECTRA BY MULTIPLE FOIL ACTIVATION		 59
4.1	SAND-II code	59
4.1.1	SAND-II code installation	60
4.2	Energy representation in ENDF and SAND-II Libraries	61
4.3	On the choice of cross-section libraries	61
4.4	Data preparation and format for SAND-II execution	63
4.4.1	Preparation of the cross-section library tape	64
4.4.2	Preparation of the spectral activities data	64
4.4.3	Preparation of the reference spectrum data library	65
4.4.4	Preparation of SAND-II code input file	66
4.4.4.1	SAND-II input file	68

4.4.4.2	Data processing using SAND-II code	69
4.4.4.3	SAND-II output file	71
4.4.4.4	Discarded foils	75
4.5	Solution spectrum smoothing	76
4.6	Reliability of SAND-II method	80
4.7	Possible sources of errors in SAND-II method	81
 CHAPTER 5: CHARACTERIZATION OF THE NEUTRON FLUX ACROSS THE REACTOR THERMAL COLUMN USING MONTE CARLO METHOD		 83
5.1	RTP geometry	83
5.2	Reactor core	84
5.2.1	Reactor core components	85
5.2.2	Reactor core homogenization	87
5.3	Thermal column and adjacent geometry	95
5.4	Low importance surroundings	96
5.5	Monte Carlo simulation of the RTP	97
5.5.1	MCNP input files	97
5.5.1.1	Flux calculation input file	98
5.5.1.1.1	Surface cards	99
5.5.1.1.2	Cell cards	99
5.5.1.1.3	Data cards	100
5.5.1.1.3.1	Variance reduction techniques	104
5.5.1.2	Radiation dosimetry in a head phantom input file	106
5.5.1.2.1	Surface Source Write (SSW) input file	107
5.5.1.2.1.1	Surface cards	107
5.5.1.2.1.2	Cell cards	108
5.5.1.2.1.3	Data cards	108
5.5.1.2.2	Surface Source Read (SSR) input file	109
5.5.1.2.2.1	Surface cards	111
5.5.1.2.2.2	Cell cards	111
5.5.1.2.2.3	Data cards	111
5.5.1.3	Suggested modification of the thermal column input file	112
5.5.1.3.1	Surface cards	112

5.5.1.3.2	Cell cards	113
5.5.1.3.3	Data cards	113
5.5.2	MCNP output files	114
5.5.2.1	Flux calculation output file	114
5.5.2.2	Radiation dosimetry in a head phantom output file	117
5.5.2.2.1	Surface Source Write (SSW) output file	117
5.5.2.2.2	Surface Source Read (SSR) output file	121
5.5.2.2.3	Efficiency of a second-step run for neutron and gamma results	123
5.5.2.3	Suggested modification for the thermal column output file	128
5.5.3	Relative errors and statistical checks	129
CHAPTER 6: RESULTS AND DISCUSSION		134
6.1	Measured saturation activity along the thermal column	134
6.2	Neutron flux along the thermal column	138
6.2.1	Measured neutron flux along the thermal column	138
6.2.1.1	Measured total neutron flux along the thermal column	139
6.2.1.2	Measured differential neutron flux along the thermal column	141
6.2.2	MCNP calculated neutron flux along the thermal column	145
6.2.2.1	MCNP calculated total neutron flux along the thermal column	145
6.2.2.2	MCNP calculated differential neutron flux along the thermal column	149
6.3	MCNP calculated photon flux along the thermal column	154
6.3.1	MCNP calculated total photon flux along the thermal column	154
6.3.2	MCNP calculated differential photon flux along the thermal column	158
6.4	Neutron and photon flux and the BNCT requirements	159
6.5	Neutron and gamma dosimetry in a head phantom	163
6.6	Suggested modification for the thermal column	170
CHAPTER 7: CONCLUSION AND FUTURE WORK		175
7.1	Conclusion	175

7.2	Recommendations for future work	178
	REFERENCES	179
	APPENDICES	186

LIST OF TABLES

	Page	
3.1	Foil materials specifications	22
3.2	List of the calibration sources used and their parameters.	44
3.3	Concentration of impurities in polyethylene vials.	50
4.1	The identification key parameters for each cross section library chosen.	59
4.2	List of variables used in the SAND-II code input file for each measurement position.	69
4.3	Percentage deviation of the total flux at different degrees of smoothing from the total flux without smoothing.	77
5.1	Homogenization parameters for Region I of the RTP core.	92
5.2	Total and percentage weight of all elements in Region I.	92
5.3	Homogenization parameters for Region II of the RTP core.	93
5.4	Total and percentage weight of all elementals in Region II.	93
5.5	Homogenization parameters for Region III of the RTP core.	94
5.6	Total and percentage weight of all elements in Region III.	94
5.7	Summary of the sources of neutron particles creation and loss in the flux calculation run.	115
5.8	Summary of the sources of neutron particles creation and loss in SSW run.	118

5.9	Summary of the sources of gamma rays creation and loss in SSW run.	118
5.10	Summary of the sources of neutron particles creation and loss in SSR run.	121
5.11	Summary of the sources of gamma rays creation and loss in SSR run.	122
5.12	Summary of the sources of neutron particles creation and loss in the suggested modification run.	128
5.13	Summary of the sources of gamma rays creation and loss in the suggested modification run.	129
6.1	Infinitely dilute foil activity for all foils used in the measurements in units of Becquerel (Bq).	135
6.2	Total neutron flux along the thermal column calculated using SAND-II code.	140
6.3	Measured neutron flux along the thermal column divided into thermal, epithermal and fast neutron components.	143
6.4	Total neutron flux along the thermal column calculated using MCNP code.	146
6.5	Calculated neutron flux along the thermal column divided into thermal, epithermal and fast neutron components.	152
6.6	Total photon flux along the thermal column calculated using MCNP code.	155
6.7	Measured and calculated total neutron flux along the central stringer of the thermal column	161

6.8	The modified total neutron flux calculated using MCNP code	170
6.9	Modified neutron flux along the thermal column divided into thermal, epithermal and fast neutron components, calculated using MCNP code.	174

LIST OF FIGURES

	Page
2.1 Comparison of flux depth distribution for thermal and epithermal neutrons (International Atomic Energy Agency, 2001)	8
3.1 Schematic diagram of the Malaysian TRIGA Mark-II reactor.	15
3.2 Graphite pile of stringers from the thermal column door side.	15
3.3 Schematic drawing of the removable stringers in the thermal column.	16
3.4 Energy responses of foils used in the measurements.	20
3.5 Mettler Toledo® microbalance.	32
3.6 Polyethylene vials used for irradiation and counting, cadmium tube and disc cover and disc-shaped indium wire.	33
3.7 Gamma ray detection system	37
3.8 A: NaI(Tl) detector setup with lead wall shielding and NIM bin including high voltage power supply and amplifier; B: top part of the detector with a foam spacer as a source site.	40
3.9 HPGe ORTEC® detector set up horizontally with the measurement positions are punched through a perspex plastic holder circled in red and blue markers.	42
3.10 Source-detector layout; NaI(Tl) vertically and HPGe horizontally.	43
3.11 Absolute efficiency E_{abs} for the NaI(Tl) detector at different distances.	45

3.12	Absolute efficiency E_{abs} for the HPGE detector at different distances.	45
3.13	Gamma spectrum of the irradiated polyethylene vial counted for four days after irradiation.	50
4.1	Measured to calculated activity ratio for all reactions obtained from the second run for spectrum 19	70
4.2	The reference spectrum used in input file 19.	74
4.3	The solution integral spectrum at position 19.	74
4.4	The solution differential spectrum at position 19.	75
4.5	Solution differential spectrum at position 19 at 40 smoothing degrees.	77
4.6	Reference spectrum generated using MCNP, SAND-II solution spectrum without smoothing and manually smoothed solution spectrum that is considered the real solution spectrum.	79
5.1	RTP homogenized core shows the three homogenized regions with other non-homogenized parts with the neutron importance reference colors displayed (produced from Monte Carlo simulation, not scaled).	89
5.2	Vertical cross section of the RTP simulated components with the neutron importance reference colors displayed (produced from Monte Carlo simulation, not scaled).	95
5.3	Horizontal cross section of the RTP simulation with the surface numbers displayed and the color reference is the material.	98
5.4	Reference neutron spectrum of Am-Be source used in RTP core (Lorch, 1973)	102

5.5	Vertical cross section of the RTP simulation with the head phantom and surface 240 displayed and the color reference is the neutron importance.	106
5.6	Vertical cross section of the RTP simulation with the color reference is the neutron importance.	110
5.7	Vertical cross section of the RTP simulation shows the cone covered from inside with a layer of bismuth followed by a layer of lead. Color refers to the material.	113
5.8	A: Comparison of the normalized neutron flux at the surface of detector 31 obtained from the SSW and SSR runs. B: Comparison of the normalized neutron dose to detector 31 obtained from the SSW and SSR runs.	126
5.9	A: Comparison of the normalized photon flux at the surface of detector 31 obtained from the SSW and SSR runs. B: Comparison of the normalized photon dose to detector 31 obtained from the SSW and SSR runs.	127
6.1	Measured activity of As, Au and Co and their cadmium-covered results along the central stringer G7.	138
6.2	Measured total neutron flux along the central stringer of the thermal column.	140
6.3	Measured differential neutron flux for positions 6, 12, 18, 19-31, 37, 43 and 49 along the thermal column.	141
6.4	Measured neutron spectrum components. A: Thermal neutron component, B: Epithermal neutron component and C: Fast neutron component.	144

6.5	Total neutron flux for positions 1 through 49 along the thermal column calculated using MCNP code.	147
6.6	Calculated total neutron flux mapping along the thermal column. A: innermost positions. B: outermost positions.	149
6.7	Calculated differential neutron flux for positions 6, 12, 18, 19-31, 37, 43 and 49 along the thermal column.	150
6.8	MCNP Calculated neutron spectrum components. A: Thermal neutron component, B: Epithermal neutron component and C: Fast neutron component.	153
6.9	Total photon flux for positions 1 through 49 along the thermal column calculated using MCNP code.	156
6.10	Total photon flux mapping along the thermal column. A: innermost positions. B: outermost positions.	157
6.11	Calculated differential photon flux for positions 6, 12, 18, 19-31, 37, 43 and 49 along the thermal column.	159
6.12	MCNP calculated results versus the measured results with a straight-line representation of the results.	160
6.13	Measured and calculated total neutron flux along the central stringer of the thermal column.	162
6.14	3-D view of the neutron relative dose along the central horizontal slice of the water phantom in a linear scale in units of cm.	165
6.15	3-D view of the neutron relative dose along the central horizontal slice of the water phantom in a logarithmic scale in units of cm.	166

6.16	2-D view of the neutron isodose lines along the central horizontal slice of the water phantom in units of cm.	167
6.17	Neutron depth dose curve at the central line of the head phantom normalized to the maximum relative dose	168
6.18	Gamma depth dose curve at the central line of the head phantom normalized to the maximum relative dose	168
6.19	Neutron and gamma depth relative dose curves at the central line of the head phantom normalized to the maximum relative dose	169
6.20	Modified total neutron flux compared with the current total neutron flux, calculated using MCNP code.	171
6.21	Neutron flux gain value along the central stringer of the thermal column	172
6.22	Modified differential neutron flux along the central stringer of the thermal column calculated using MCNP code.	173

LIST OF PLATES

	Page
5.1 A: Horizontal cross-section diagram of RTP core arrangement showing the upper plate, neutron source position, Graphite reflector, thermal column and other beam ports, detector position, Water tank and other parts (RTP archive library). B: Vertical cross section diagram of the RTP core arrangement showing the upper and lower grid plates, fuel rod, rotary rack well, graphite reflector and other parts of the core (The TRADE collaboration, 2002).	86
5.2 A: Fuel-follower type control rod withdrawn and inserted compared to the fuel element fixed in position (RTP archive library). B: TRIGA standard fuel element with the stainless steel cladding and internal composition shown (RTP archive library).	89

LIST OF APPENDICES

	Page
I SAND-II code input file used for processing data of position 19	187
II SAND-II code output file for position 19	188
III Monte Carlo input file for the neutron and gamma flux calculation throughout the thermal column of the RTP reactor	193
IV Selected cards from the Surface Source Write (SSW) input file	203
V Selected cards from the Surface Source Read (SSR) input file	209
VI Selected cards from the suggested modification of the thermal column input file	211
VII Selected cards from the output file of the SSW run	214

**PENGUKURAN FLUKS NEUTRON DENGAN VERIFIKASI MONTE CARLO
PADA TURUS TERMA REAKTOR TRIGA MARK II: KAJIAN
KEBOLEHLAKSANAAN KEMUDAHAN BNCT**

ABSTRAK

Rawatan tumor otak malignan melalui Terapi Tawanan Neutron Boron (BNCT) memerlukan punca neutron dengan fluks yang tinggi. Reaktor TRIGA Mark II Malaysia diselidiki untuk pemasangan BNCT yang dicadangkan. Fluks neutron diukur sepanjang *stringer* pusat turus terma dan kedudukan paling luaran *stringer* yang lain. Kaedah *unfolding* kerajang digunakan di sini. Aluminium (Al), arsenic (As), gold (Au), cobalt (Co), indium (In), molybdenum (Mo), nickel (Ni), dan rhenium (Re), dan cadmium (Cd) sebagai penutup dengan 19 tindak balas yang berguna telah dimanfaatkan dalam kajian ini. Keaktifan kerajang yang cair secara tak terhingga dihitung dan digunakan dalam kod SAND-II (*Spectrum Analysis by Neutron Detectors*) untuk menghitung fluks neutron. Reaktor tersebut juga disimulasi menggunakan kod Monte Carlo (MCNP5) dan fluks neutron dihitung sepanjang turus terma. Fluks neutron yang diukur dan dihitung sepanjang turus terma menunjukkan persetujuan yang baik. Keperluan keamatan neutron epiterma minimum yang diperlukan untuk BNCT dicapai sehingga kedudukan 22 dengan alur neutron-gamma bercampur. Pengubahsuaian turus terma reactor yang dicadangkan melalui simulasi MCNP meningkatkan fluks neutron pada jarak yang jauh dari teras reactor tetapi bahagian neutron epiterma lebih rendah dari keperluan minimum pemasangan BNCT. Perhitungan fuks foton di sepanjang turus terma menunjukkan keputusan yang agak tinggi yang perlu ditapis. Perhitungan dos neutron dan dos gama dalam fantom kepala (air) menunjukkan bahawa spektrum neutron

yang sedia ada memerlukan pengubahsuaian untuk meningkatkan bahagian neutron epiterma dan menapis kontaminasi sinar gama.

NEUTRON FLUX MEASUREMENTS WITH MONTE CARLO VERIFICATION AT THE THERMAL COLUMN OF A TRIGA MARK II REACTOR: FEASIBILITY STUDY FOR A BNCT FACILITY

ABSTRACT

The treatment of the malignant brain tumor through Boron Neutron Capture Therapy (BNCT) requires a high-flux neutron source. The Malaysian TRIGA Mark II reactor was investigated for a proposed BNCT facility. The neutron flux was measured along the central stringer of the thermal column and the outermost positions of the other stringers. The unfolding foil method was applied here. The aluminum (Al), arsenic (As), gold (Au), cobalt (Co), indium (In), molybdenum (Mo), nickel (Ni) and rhenium (Re) foils, and cadmium (Cd) as a cover were used with 19 useful reactions in this study. The infinitely diluted foil activity was calculated and used in the Spectrum Analysis by Neutron Detectors (SAND-II) code to calculate the neutron flux. The reactor was also simulated using Monte Carlo code (MCNP5) and the neutron flux was calculated along the thermal column. The measured and calculated neutron flux along the thermal column show good agreement. The minimum epithermal neutron intensity required for BNCT is achieved up to position 22 with a mixed neutron-gamma beam. A suggested MCNP simulated modification of the reactor thermal column increased the neutron flux at distant positions from the reactor core but the epithermal neutron part was below the minimum requirement for a BNCT facility. The photon flux calculations along the thermal column show relatively high results which should be filtered. The calculation of the neutron and gamma dose in a head phantom (water) indicated that the available neutron spectrum requires modifications to increase the epithermal part of the neutrons and filter the gamma ray contamination in order to be used for BNCT facility.

CHAPTER 1

INTRODUCTION

The huge increase in the number of the glioblastoma multiforme brain tumors encourages scientists to investigate more methods in treating this malignant tumor. It is usually fatal within six months of diagnosis even with available standard treatment (International Atomic Energy Agency 2001). An efficient treatment for the brain tumor requires highly selective destruction of tumor cells with minimal destruction to the healthy cells spread among or hosting the tumor. For this purpose, the technique of Boron Neutron Capture Therapy (BNCT) has been further developed.

The penetration of the neutron depends mainly on its energy. The penetration of thermal neutrons is relatively limited and it accumulates a dose peak in a depth close to the surface. The use of an epithermal neutron beam shifts the peak dose to an increased depth (Wheeler *et al.*, 1990). The main source extensively used for the purpose of BNCT is the nuclear reactor. Generally, the neutron quality in the neutron beam requires modifications to provide the suitable neutron energy and flux for such BNCT facilities.

In this study, the measurements of the neutron flux along the thermal column of the Malaysian TRIGA (Training, Research, Isotopes, General Atomic) Mark-II PUSPATI research reactor (RTP) were performed. The measurements include all the positions in the central stringer and the outermost positions of the other stringers. The unfolding foil method was applied in this study. A set of eight pure

foil materials is activated using the neutron flux in the thermal column. Aluminum (Al), arsenic (As), gold (Au), cobalt (Co), indium (In), molybdenum (Mo), nickel (Ni) and rhenium (Re) foils and cadmium (Cd) as a cover were used in this study with 19 useful reactions. The activity is measured for each foil and the neutron flux is calculated from this activity. The Sodium-Iodide-Thallium (NaI(Tl)) and the High-Purity Germanium (HPGe) radiation detectors for this purpose.

The SAND-II code (Spectrum Analysis by Neutron Detectors, Los Alamos national laboratory (2003)) was used to calculate the neutron flux along the thermal column using the foil-activity results. All cross-section libraries were downloaded from the National Nuclear Data Center (NNDC) worldwide page (Evaluated Nuclear Data File, ENDF).

The reactor core and thermal column including the surrounding geometry were simulated using the Monte Carlo N-particle (MCNP5, Los Alamos national laboratory (2005)) simulation code. A number of variance reduction techniques were used in the simulation. The components of the reactor core were substituted with an equivalent homogenous mixture to simplify the simulation.

The neutron and photon total and differential flux were calculated along the thermal column of the reactor using the MCNP code. The neutron and gamma relative dose in a water head phantom were then calculated. Calculations of the neutron and photon total and differential flux were also calculated for a proposed modification of the thermal column.

The neutron flux measurements were performed with many limitations and obstacles. The difficulty in inserting wires and probes into the measurement positions for direct-measurement detectors and the difficulty of using liquid or volatile-product isotopes limited the choice of the neutron detectors. The reactor operating schedule and the appropriateness of the irradiation power and time added more difficulties to the practical measurements schedule. The limited number of users of the SAND-II code and the difficulty of processing the huge cross-section files delayed the production of the practical results.

The objectives of this study can be summarized as follows:

- To measure the neutron spectra along the thermal column of the Malaysian TRIGA Mark II reactor.
- To calculate the neutron spectra along the thermal column of the reactor using MCNP code.
- To compare the measured and calculated neutron spectra at the thermal column of the reactor.
- To determine and characterize the gamma rays associated with the neutron spectra along the thermal column using MCNP code.
- To study the relative depth dose profile from neutrons and gamma rays in a water head phantom using MCNP code.
- To propose and test modifications to the thermal column to comply with the requirements for a suggested BNCT facility using MCNP code.

An introductory review of BNCT, SAND-II and MCNP was presented in Chapter 2. The measurements of the neutron flux along the central stringer of the thermal column and the outermost positions of the other stringers were explained in Chapter 3. Chapter 4 explained the analysis of the neutron flux using SAND-II code, while Chapter 5 covered the MCNP simulation of the thermal column of the reactor, the water head phantom and proposed modifications to the thermal column. Chapter 6 covered the analysis and discussion of the measurements and MCNP simulation results. It also covered the MCNP simulation results of gamma and neutron dosimetry in the head phantom, while Chapter 7 summarizes the conclusions of this study.

CHAPTER 2

INTRODUCTORY REVIEW

2.1 BNCT - Historical review

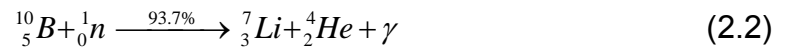
Neutron Capture Therapy (NCT) was first proposed by Locher in 1936 (Laramore *et al.*, 1994) when he proposed treating tumors with thermal neutrons and utilizing Boron-10 (^{10}B) which has a high reaction cross section. Sweet (1951) realized the clinical potential of BNCT in treating brain tumors. Sweet and colleagues (Barth *et al.*, 1994) directed their work towards treating patients using different boron compounds. None of the used compounds show tumor selectivity, which caused damage to healthy and tumor cells of the brain.

It was in the mid-1960s when Hatanaka discovered the sodium borocaptate (BSH) compound, which appeared to have tumor localizing properties (Soloway *et al.*, 1967). After his return to Japan from USA in 1965, Hatanaka (1975) initiated a clinical trial with a combination of surgery and BNCT using the BSH compound. Although his patients had either deeply seated or recurrent tumors, Hatanaka's results have stimulated interest in BNCT. The use of nuclear reactors for BNCT did not limit the interest or the controversy towards BNCT.

2.2 Theory of BNCT

In the BNCT technique, the patient is injected with a boron-10 (^{10}B) carrier compound, which has the ability to trace tumor cells and accumulate

therein. After a certain time (30 minutes to 2 hour), the boron-carrier compound washes out from the body leaving a high difference in boron concentration between healthy and tumor cells (3.5:1 tumour/blood, Coderre *et al.*, 1997). The patient is then exposed to an epithermal neutron beam, which is thermalized and highly absorbed by boron. The capture of the thermal neutrons by boron leads to one of the following two reactions (Bradley *et al.*, 1999):



Both alpha and lithium are high LET (Linear Energy Transfer) particles that deposit their energies within the cell or in the maximum case to the next cell, which gives a highly localized treatment to the tumor cells and saves the healthy cells.

2.3 Neutron energy and BNCT

Neutrons interact with matter in a different way from other types of radiation. No coulomb forces with orbital electrons or the nuclei of the atom affect the neutrons, as they are considered electrically uncharged. Neutrons must either enter the nucleus or pass very close to it for the nuclear forces to act. If the nucleus of a material is excited, different types of nuclear reactions may be possible. The main factors that determine the type of nuclear reaction are the energy of the incident neutron and the composition of the absorbing

material (including the location of energy levels in the nuclei). Curtiss (1969) classified the neutrons based on their energy to 8 categories (slow, cold, thermal, epithermal, resonance, intermediate, high energy and ultra high energy neutrons). Profio (1976) classified neutrons based on their energy to three general categories:

- 1- Thermal neutrons: they are those that have reached thermal equilibrium with their surroundings.
- 2- Epithermal neutrons: they are those between thermal and fast neutrons, above 1 eV and below 1 keV.
- 3- Fast neutrons: they are those with a lower energy-boundary of about 100 keV.

According to their effect and application in BNCT treatment, the standard classification of the neutrons is different from others as follows (International Atomic Energy Agency, 2001):

- 1- Thermal neutrons: neutrons with energy up to 0.5 eV.
- 2- Epithermal neutrons: neutrons within energy range of 0.5 eV and 10 keV.
- 3- Fast neutrons: neutrons with energy higher than 10 keV.

In BNCT, the ideal neutron beam has to create an adequate thermal neutron field in the prescribed tumour volume. This means that the neutron beam has to be optimized according to the depth of the tumour volume in the patient. Figure

2.1 (International Atomic Energy Agency, 2001) compares the flux depth for thermal and epithermal neutrons in phantom. The maximum thermal neutron flux is achieved at the surface (skin) and drops exponentially. The epithermal neutron beam creates a maximum thermal neutron flux at a depth of 2-3 cm, which drops exponentially thereafter. It is obvious that the penetration of the beam can be increased by increasing the average neutron beam energy. It can also be increased by increasing the forward direction of the beam with smaller beam sizes (International Atomic Energy Agency, 2001).

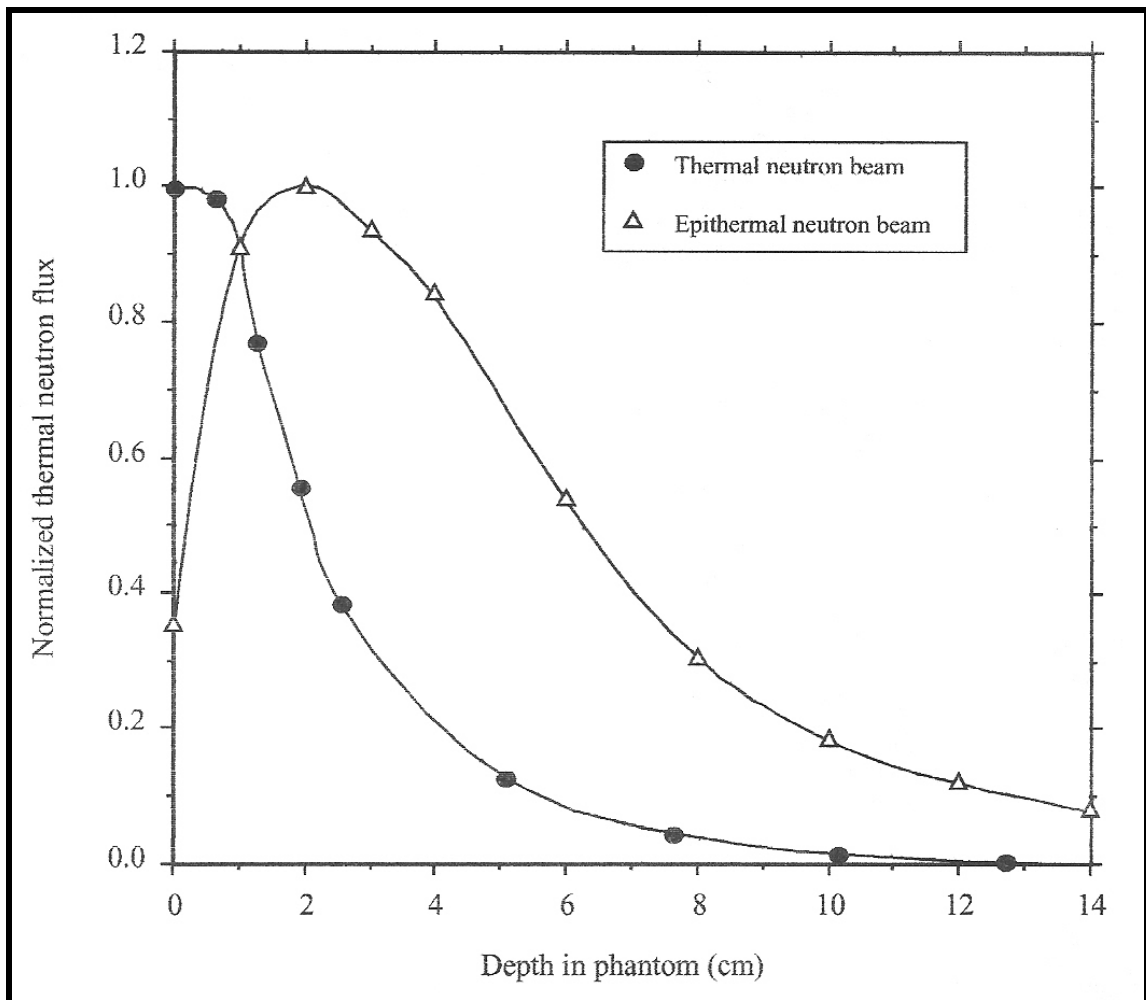


Figure 2.1 Comparison of flux depth distribution for thermal and epithermal neutrons (International Atomic Energy Agency, 2001).

2.4 BNCT - Increased interest and more facilities

After the achievement of Hatanaka in the BNCT technique (Hatanaka, 1975), the interest increased in the BNCT technique with more support to all aspects of the treatment. After the first human trial of BNCT in the United States, and the successful human trials at Hitachi Training Reactor (HTR) facility in Japan, the neutron irradiation facility at the Japan Research Reactor-3 (JRR-3) facility was used for the same purpose followed by the Musashi Institute Reactor (MulTR) facility (Nakagawa, 2006). The trials were resumed in the United States at the Massachusetts Institute of Technology (MIT) and at Brookhaven National Laboratory (BNL) (Nigg, 2006). The earlier trials were using thermal energy neutrons that require the removal of the scalp and the skull prior to irradiation to deposit the radiation dose to deeper-seated tumors without damage to the scalp while the latter trials utilized an epithermal neutron beam.

Trials for BNCT have been initiated in some other reactors in Japan and the United States as well as Europe and South America. Feasibility studies and clinical trials are currently continuing in Japan, Finland, the Netherlands, the Czech Republic, Italy and Argentina (Nigg, 2006), Taiwan (Chou *et al.*, 2006), Iran (Pazirandeh *et al.*, 2006), Ukraine (Gritzay *et al.*, 2006), Morocco, Thailand, Indonesia, Kazakhstan, Sweden (International Atomic Energy Agency, 2001) and Malaysia.

As an alternative neutron source for the reactors, accelerator-based neutron sources were investigated for the BNCT technique such as those at the University of Washington and the Fermi National Accelerator Laboratory in the United States and in Essen, Germany as well as in France (Nigg, 2006). Many other institutes and hospitals have launched studies concerning the accelerator-based BNCT facility such as other universities and institutes in the United States, Canada, the United Kingdom, Russia, Japan, Switzerland, Italy, Australia, Germany, Korea, China, Argentina and other countries (Nigg, 2006, Blue *et al.*, 2003).

2.5 The SAND-II choice

The gold foil method is used for the neutron flux measurement. This method utilizes the reaction of ^{197}Au with neutrons to produce ^{198}Au . This method is useful in the measurement of the neutron flux within certain allowed error. The more accurate method is the unfolding foil method where many pure metals are used to measure the neutron energy flux. The latter method involves more pure metals and gives much more information, which gives higher accuracy to the measured flux.

The unfolding foil method uses a program to calculate the neutron energy flux from the activity of the foils. The MAXED code is used to unfold the neutron flux from the results of “few channels” or detectors. It is part of the U_M_G (Unfolding MAXED GRAVELL) batch contributed by the PTB (Physikalisch-

Technische Bundesanstalt, Germany). The MAXED code cannot be used in this study due to the limited number of detectors used for this code.

The GRAVELL code is used to unfold the neutron flux from the results of “multiple channels” or detectors. It is another part of the U_M_G batch. The GRAVELL code is a modified version of the SAND-II (Spectrum Analysis by Neutron Detectors) code. The modified version is easier to use but limited in less number of applications. The GRAVELL code showed more difficulties in setting the response table for each foil. The trials stopped after the code failed to accept the provided response table (Reginatto, 2006).

The SAND-II code (Oak Ridge National Laboratory) uses an iterative perturbation method to obtain a best-fit neutron flux spectrum. The code requires an initial neutron spectrum and measured activity of foils activated by the neutron beam under investigation. The initial neutron spectrum should be chosen carefully considering a prior knowledge of the real neutron spectrum of the reactor in order to achieve closer results to the real neutron spectrum solution.

The SAND-II code includes more sub-codes and requires more preparation for each run than the GRAVELL code. The SAND-II code was successfully utilized in this study in calculating the neutron flux from the measured foil activity.

2.6 Monte Carlo technique

MCNP is a general – purpose Monte Carlo N – Particle code that can be used for neutron, photon, electron, or coupled neutron/photon/electron transport (X-5 Monte Carlo Team 2003A). It has advantages and disadvantages compared with other deterministic methods (Brugger *et al.*, 1990B). One of the disadvantages of Monte Carlo is that the result depends critically on the number of particles scored in the cell. Another disadvantage is the splitting and Russian roulette in which the particles are killed or allowed to pass through the boundary between two cells with increased or decreased weight. Improvements in the variance are gained by transporting more particles.

One of the important advantages of Monte Carlo is that it employs the point energy data so that each particle is tracked using interaction cross-section data appropriate to its actual energy. Another advantage of the Monte Carlo is its ability to simulate sophisticated shapes and to import geometries from other programs.

Monte Carlo technique is used in medical physics with increasing interest. It was used in brachytherapy calculations, radiation dosimetry, stopping-power ratio, wall attenuation corrections for primary standards of air kerma, modeling radiotherapy beams, treatment planning, BNCT and many other aspects (Rogers, 2006).

2.7 Head phantom and BNCT dosimetry

The characterization of the neutron beam for dosimetry in BNCT is important. Different phantom materials were suggested for this purpose. Polymethylmethacrylate (PMMA) and water were considered good phantom materials for BNCT in epithermal beams (Seppala *et al.*, 1997). Raaijmakers *et al.* (1995) used polyethylene and water phantoms in the measurement of neutron dose from the HFR (High Flux Reactor) in The Netherlands.

Some research groups mixed water with different amounts of boron-10 (Brugger *et al.*, 1990A), while others mixed water with different amounts of Nitrogen-14 for the purpose of thermal neutron dosimetry. In this study, cylindrical-shape water phantom was simulated using Monte Carlo code to calculate the neutron and gamma dose in a head-like phantom.

CHAPTER 3

NEUTRON BEAM MEASUREMENTS USING FOIL ACTIVATION METHOD

3.1 TRIGA Mark II Reactor

The TRIGA Mark-II PUSPATI Research Reactor (RTP), the only reactor available in Malaysia, started operations in the year 1982. It is a pool type reactor with demineralized light water as moderator, high purity graphite as a reflector and uranium-235 as a fuel. The reactor is mainly devoted to research, development, training and education purposes.

The RTP power capacity is 1 MW in the steady state with an average neutron flux of $1.2 \times 10^{12} \text{ cm}^{-2} \text{ s}^{-1}$. It uses the standard TRIGA fuel element as its nuclear fuel. The reactor has two radial beam ports, one radial piercing beam port, one tangential beam port and the graphite thermal column as shown in Figure 3.1. It produces neutrons with energies up to 10 MeV. More details about the reactor core and thermal column are available in Chapter 5.

3.1.1 Graphite Thermal Column

The thermal column of the RTP is divided into two parts; the inner part of the graphite which is right at the peripheral of the graphite reflector, and the second part which is the outer part right behind the door of the thermal column. The outer part is a pile of graphite stringers stacked in layers crossway and along the thermal column (Figure 3.2). The stringers measure 10.16×10.16

cm² with length of 127 cm except for the lower most and the upper most layers which measure 10.16 x 3.18 cm² with the same length.

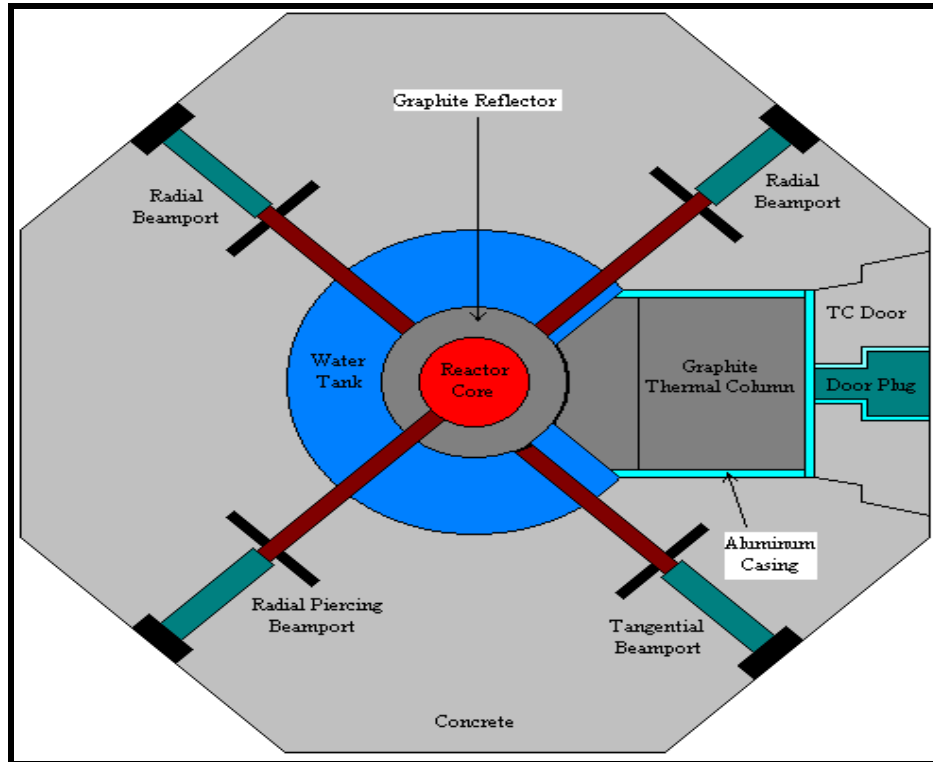


Figure 3.1 Schematic diagram of the Malaysian TRIGA Mark-II reactor.

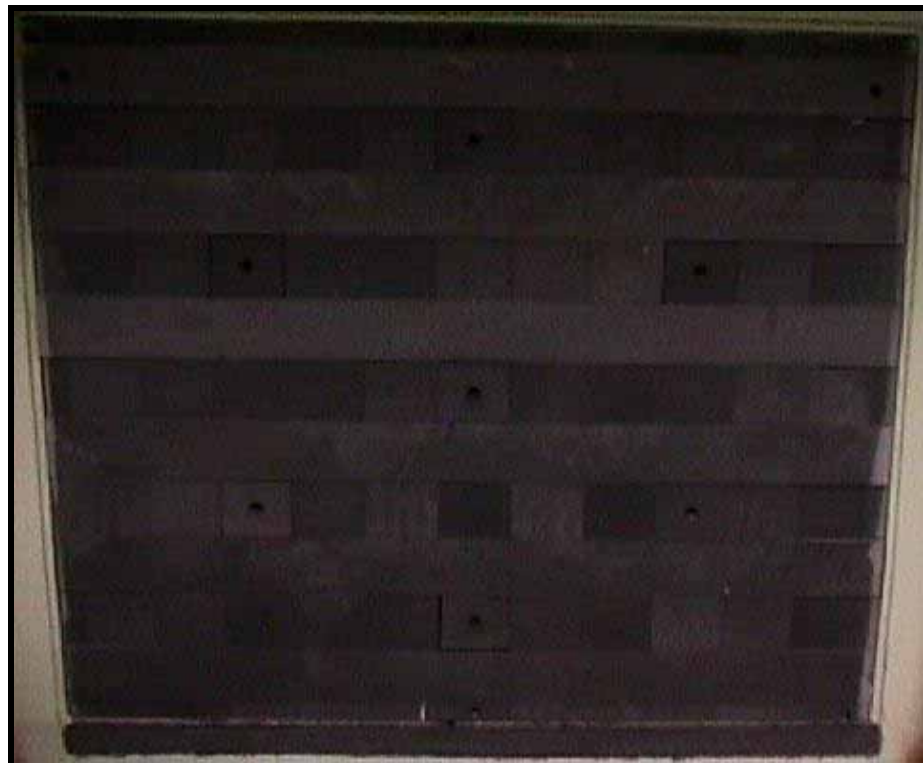


Figure 3.2 Graphite pile of stringers from the thermal column door side.

The graphite stringers are labeled according to their position starting from the lower most row with label A, up to the upper most row with label N with the letter I skipped. Figure 3.3 shows a drawing of the removable seven stringers of the thermal column labeled according to their positions. Six of these stringers are provided with six holes of about 2 cm diameter and 0.7 cm depth with spacing of about 24.5 cm from each other for the purpose of sample irradiation inside the thermal column. The central stringer labeled G7 contains the most number of holes (13 holes) with spacing of about 10 cm from each other. This is because the neutron flux is the highest through this stringer and more measurement points are required in evaluating the neutron flux at that stringer. The holes of all stringers are numbered starting from innermost holes and going outwards far from the core and from the lower most stringer and going upwards. The choice of numbering was made in order to simplify the description of the experiments.

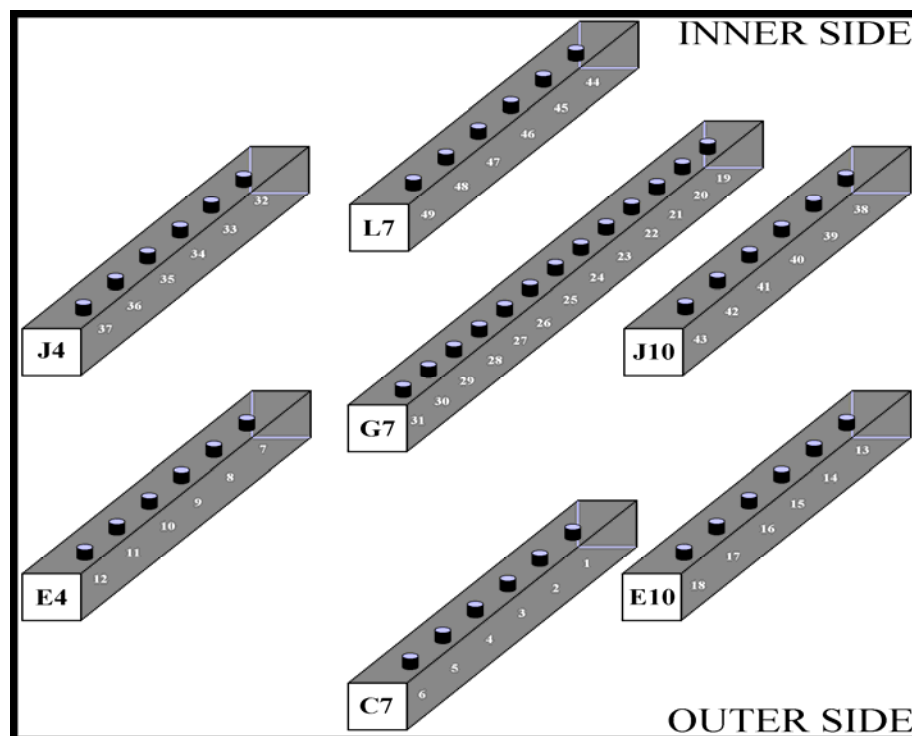


Figure 3.3 Schematic drawing of the removable stringers in the thermal column.

3.2 Measurement of the neutron flux density in the thermal column

In order to measure the neutron flux density in the thermal column the foil activation method was used. Foils have many advantages over other types of detectors; such as:

- 1- Relatively cheap in price.
- 2- Small size, can be put in small positions and can be easily shaped.
- 3- Insensitive to gamma rays.
- 4- Independent of electrical connections.
- 5- Adaptive to different environments.
- 6- Easy to handle.

3.2.1 Selection criteria of activation foils

Many factors should be considered in selecting the activation foil set. The following factors were considered in the selection:

- 1- The energy response of the whole set covers most of the neutron spectrum.
- 2- The dominant energy of the neutron flux at different positions along the thermal column.
- 3- The cross section of the reaction. Many foils were discarded, as the activities produced were small due to their low cross section value.
- 4- The irradiation time and half-life of the product isotope. Irradiation time was fixed to 6 hours, which required foils with high cross

section to be used in order to achieve reasonable counting rates within this time. The half-life of the product isotope should not be very long because it is inversely proportional to the activity of the product isotope. Relatively long half-life reaction products were used as the removal of the samples from the thermal column was scheduled the day following the irradiation.

- 5- The irradiation environment affects some types of foils that are highly sensitive to humidity and high temperature or strong reactions with air contents. None of these foils were used.
- 6- The type and energy of the emitted radiation from the samples. In this study the emitted gamma rays from the activated foils were studied. The advantages of gamma ray are well known in terms of low effect by self-absorption and backscattering in the foil. Beta particles were not detected in this study. Reactions which produced very low-energy gamma rays were also discarded.
- 7- Interfering activities of impurities. A purity of 99.9+% was maintained for the foils used in order to eliminate the effect of this factor.
- 8- Foils chosen were easy to fabricate and shape following the irradiation position geometry.
- 9- Solid metallic and powder materials were used. Liquid materials were not used according to the safety rules of the reactor.

3.2.2 Foil energy-response

As mentioned above, foils were selected according to their response to the energy of the neutrons. The cross-section data of different materials were studied (Baard *et al.*, 1989). Cross-section data for the MTR (light water Material Testing Reactor) was considered, as it is the nearest representation of TRIGA reactors. Figure 3.4 represents 90% of the energy response of each foil used, obtained from Baard *et al.*, (1989). The remaining 10% is divided into two halves, 5% below the plotted range and 5% above it. The black line represents the median of the energy response for each foil, which indicates the energy for which the responses below and above this energy are equal. The cross-section data in Figure 3.4 were based on ENDF/B-V file while more recent cross-section libraries were used in SAND-II. This energy response range covers most of the neutron spectrum from below 0.01 eV up to about 10 MeV. Revisions of the ENDF/B-V file are not expected to significantly alter Figure 3.4.

3.2.3 Foil testing

A set of twenty foils available in the laboratory was tested using X-ray fluorescence (XRF) to confirm the type and purity of the materials. These foils were then tested in the reactor's thermal column in the inner most positions 1, 7, 13, 19, 32, 38 and 44. The aim of this test was to initially study the neutron flux and the efficiency of using these detectors in this study. The foils tested in the thermal column were silver (Ag), aluminum (Al), arsenic trioxide (As_2O_3), gold (Au), cobalt (Co), copper (Cu), iron (Fe), indium (In), molybdenum (Mo), niobium (Nb), nickel (Ni), palladium (Pd), rhenium (Re), tin (Sn), tantalum (Ta),

titanium (Ti), standard uranium ORE (U_3O_8 , distributed by the International Atomic Energy Agency (IAEA)), tungsten (W), zinc (Zn) and zirconium (Zr). Cadmium (Cd) was studied as well and used as an absorber for the thermal neutrons (cover material). Many of these foils were not used as they did not fulfill one or more of the foil selection criteria mentioned above. The foils finally selected in this study were Al, As, Au, Co, In, Mo, Ni, Re and Cd as a cover.

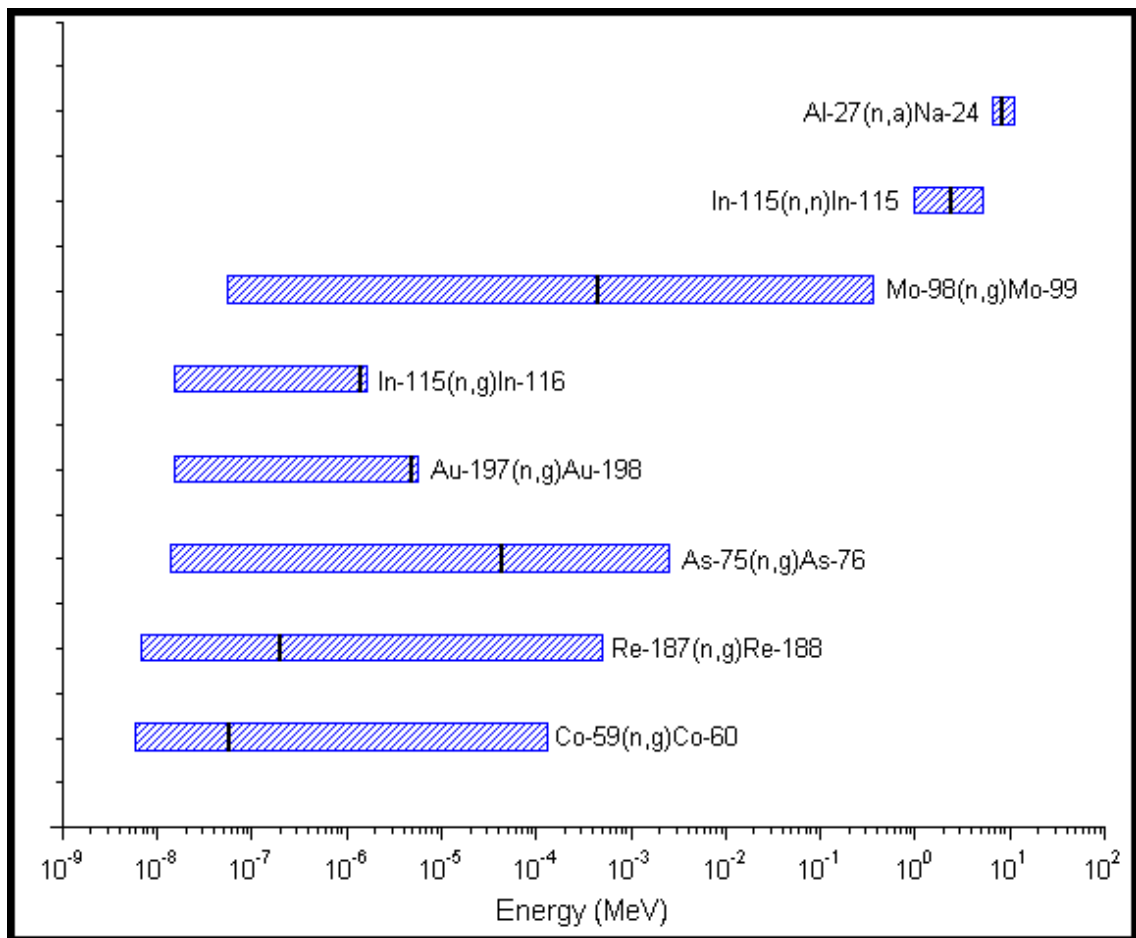


Figure 3.4 Energy responses of foils used in the measurements.

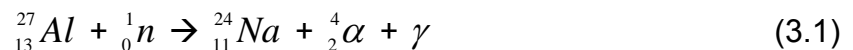
3.2.4 Foils used in the experimental work

As mentioned previously, eight foil materials were selected for the experimental work. Each material has different cross-sections and gamma

energy emissions. Many of these materials have many reactions following their different isotopes naturally available together. The reactions of each isotope were studied and the useful isotope reactions were selected. A study of all foils used, their major possible reactions, reactions accepted and reactions rejected are summarized in this section. Table 3.1 also includes some properties of the materials used such as: purity, impurities present, foil shape, foil thickness for foils, diameter for wires, wall thickness for tubes, studied isotopes, natural abundance of each isotope, product isotope after reaction with neutrons and product isotope half life.

3.2.4.1 Aluminum (Al)

Aluminum has one stable isotope ($^{27}_{13}\text{Al}$) (Browne *et al.*, 1986). The following reaction was used and the activity of $^{24}_{11}\text{Na}$ isotope was measured.



In this reaction, $^{27}_{13}\text{Al}$ captures a neutron forming $^{28}_{13}\text{Al}$ which transforms into $^{24}_{11}\text{Na}$ liberating ${}^4_2\alpha$ particle with gamma ray of energy peaks of 1368.598 keV and 2753.995 keV. Measurements were done in holes 19 – 22 of the central graphite stringer with bare aluminum only with no detectable activity observed beyond position 22.

3.2.4.2 Arsenic (As)

Arsenic has one stable isotope ($^{75}_{34}\text{As}$) (Browne *et al.*, 1986). It was utilized in the form of a powder compound of arsenic trioxide (As_2O_3). The following reaction was used and the activity of $^{76}_{34}\text{As}$ was measured.



In this reaction, $^{75}_{34}\text{As}$ captures a neutron forming $^{76}_{34}\text{As}$ which decays with gamma ray energy emissions at 559.08 keV and 563.27 keV. Measurements were done in holes 6, 12, 18, 19-31, 37, 43 and 49 of the graphite stringers with bare as well as cadmium-covered arsenic.

3.2.4.3 Gold (Au)

Gold has one stable isotope ($^{197}_{79}\text{Au}$) (Browne *et al.*, 1986). The following reaction was used and the activity of $^{198}_{79}\text{Au}$ was measured.



In this reaction, $^{197}_{79}\text{Au}$ captures a neutron forming $^{198}_{79}\text{Au}$ which decays with gamma ray energy emission at 411.805 keV. Measurements were done in holes (1-49) of all the graphite stringers with bare and cadmium-covered gold. In the initial measurements the results were all rejected as the irradiated vial

containing the foils contributed some of the activity to the counting system. The experimental procedure had to be modified and the measurements were repeated in holes 6, 12, 18, 19-31, 37, 43 and 49 of the graphite stringers with bare and cadmium-covered gold foils.

3.2.4.4 Cobalt (Co)

Cobalt has one stable isotope ($^{59}_{27}\text{Co}$) (Browne *et al.*, 1986). The following reaction was used and the activity of $^{60}_{27}\text{Co}$ was measured.



In this reaction, $^{59}_{27}\text{Co}$ captures a neutron forming $^{60}_{27}\text{Co}$ which decays with gamma ray energy emissions at 1173.237 keV and 1332.501 keV. Measurements were done in holes 6, 12, 18, 19-31, 37, 43 and 49 of the graphite stringers with bare as well as cadmium-covered cobalt foils.

3.2.4.5 Indium (In)

Indium has one stable isotope ($^{113}_{49}\text{In}$) and another naturally occurring radioactive isotope ($^{115}_{49}\text{In}$, half-life 4.41×10^{14} years) with 4.3% and 95.7% natural abundance respectively (Browne *et al.*, 1986). For the stable isotope, the following reaction was used and the activity of $^{114m}_{49}\text{In}$ was measured.